LETTER

doi:10.1038/nature15695

Kidney organoids from human iPS cells contain multiple lineages and model human nephrogenesis

Minoru Takasato[1,2], Pei X. Er[1], Han S. Chiu[2], Barbara Maier[2], Gregory J. Baillie[2], Charles Ferguson[2], Robert G. Parton[2], Ernst J. Wolvetang[3], Matthias S. Roost[4], Susana M. Chuva de Sousa Lopes[4] & Melissa H. Little[1,2,5]

The human kidney contains up to 2 million epithelial nephrons responsible for blood filtration. Regenerating the kidney requires the induction of the more than 20 distinct cell types required for excretion and the regulation of pH, and electrolyte and fluid balance. We have previously described the simultaneous induction of progenitors for both collecting duct and nephrons via the directed differentiation of human pluripotent stem cells[1]. Paradoxically, although both are of intermediate mesoderm in origin, collecting duct and nephrons have distinct temporospatial origins. Here we identify the developmental mechanism regulating the preferential induction of collecting duct versus kidney mesenchyme progenitors. Using this knowledge, we have generated kidney organoids that contain nephrons associated with a collecting duct network surrounded by renal interstitium and endothelial cells. Within these organoids, individual nephrons segment into distal and proximal tubules, early loops of Henle, and glomeruli containing podocytes elaborating foot processes and undergoing vascularization. When transcription profiles of kidney organoids were compared to human fetal tissues, they showed highest congruence with first trimester human kidney. Furthermore, the proximal tubules endocytose dextran and differentially apoptose in response to cisplatin, a nephrotoxicant. Such kidney organoids represent powerful models of the human organ for future applications, including nephrotoxicity screening, disease modelling and as a source of cells for therapy.

The mammalian kidney is derived from intermediate mesoderm. Cells from the primitive streak (presomitic mesoderm; PSM) migrate rostrally to form the intermediate mesoderm[2]. The intermediate mesoderm gives rise to both key kidney progenitor populations, the ureteric epithelium and the metanephric mesenchyme, which form the collecting ducts and nephrons, respectively. Several studies have reported the successful differentiation of human pluripotent stem cells (hPSCs) into either ureteric epithelium or metanephric mesenchyme *in vitro*[3–7]. In contrast, we previously reported the simultaneous generation of both ureteric epithelium and metanephric mesenchyme from hPSCs, resulting in the induction of nephrons and collecting ducts[1]. This was paradoxical as it was assumed that the ureteric epithelium arises as a side branch of the mesonephric duct, itself forming from the anterior intermediate mesoderm, while the metanephric mesenchyme is derived from the posterior intermediate mesoderm[5,8]. Retinoic acid (RA) regulates anterior–posterior patterning in organogenesis with rostral RA signalling patterning the somites[9] (Fig. 1e). Conversely, the PSM expresses Cyp26, which attenuates RA signalling in the caudal embryo[10,11]. The PSM is also a strong site of Wnt signalling[12]. In our previous studies, we demonstrated *in vitro* that formation of the intermediate mesoderm required FGF9 or FGF2 (ref. 1). Hence, *in vivo* we assume that the ureteric epithelium forms from early migrating PSM cells exposed to FGF9 and RA soon after the primitive streak stage, while cells late to migrate, and hence exposed to longer Wnt signalling, should give rise to the metanephric mesenchyme[13] (Fig. 1a). To confirm this, we varied the duration of initial Wnt signalling (using CHIR99021, an inhibitor of GSK-3) before addition of FGF9 (Fig. 1b) and monitored markers of the anterior intermediate mesoderm and posterior intermediate mesoderm by quantitative PCR. Shorter periods of CHIR99021 application induced the anterior intermediate mesoderm markers, *LHX1* and *GATA3*, whereas longer periods increased the posterior intermediate mesoderm markers, *HOXD11* and *EYA1*, at day 7. Prolonged expression of the PSM markers, *TBX6* and *T*, after a longer period in the presence of CHIR99021 suggested a delay in FGF9-induced fate commitment (Fig. 1c), as predicted. Immunofluorescence analysis showed that a longer (or shorter) period with CHIR99021 induced less (more) anterior intermediate mesoderm but more (less) posterior intermediate mesoderm, as indicated by GATA3 and HOXD11, respectively, at day 7 of differentiation (Fig. 1d). These observations persisted after 18 days of culture, with dominant ureteric epithelium induction ($GATA3^+PAX2^+ECAD^+$) after fewer days in the presence of CHIR99021 and preferential induction of metanephric mesenchyme ($PAX2^+ECAD^-$) and its derivatives ($PAX2^+ECAD^+$) with more days in the presence of CHIR99021 (Extended Data Fig. 1a). Further, we investigated whether RA signalling also controls anterior–posterior fate patterning of the intermediate mesoderm using RA or an RA receptor antagonist, AGN193109, together with FGF9 (Fig. 1e, f). RA promoted ureteric epithelium induction, whereas AGN193109 inhibited ureteric epithelium but enhanced induction of the metanephric mesenchyme lineage (Fig. 1g and Extended Data Fig. 1b).

These results increase our understanding of embryogenesis as well as providing a method by which to modulate the relative induction of each of the two intermediate mesoderm-derived progenitor populations essential for kidney formation. As a result, we modified our existing kidney differentiation process to increase the proportion of metanephric mesenchyme formed, increase the time in 3D culture and actively trigger nephron formation. This optimized approach was applied to either human embryonic stem (ES) cells or human induced pluripotent stem (iPS) cells and involved an initial 4 days of CHIR99021, which resulted in the induction of both the ureteric epithelium and the metanephric mesenchyme in monolayer culture (Extended Data Fig. 2), followed by 3 days of FGF9 before transfer to organoid culture (Fig. 2a). The resulting aggregates were cultured for up to 20 days, during which time they spontaneously formed complex kidney organoids (Fig. 2b). During normal mouse kidney development, nephron formation from the metanephric mesenchyme is initiated in response to Wnt9b secreted from the ureteric epithelium. In the mouse, ectopic nephron formation can be triggered via the addition of canonical Wnt agonists[14]. Indeed, maximal nephron number per organoid required a pulse of CHIR99021 for one hour after forming a pellet (Fig. 2a and Extended Data Fig. 3a). In addition, the continued presence of FGF9 after this CHIR99021 pulse was essential

[1]Murdoch Childrens Research Institute, The Royal Children's Hospital Melbourne, Parkville, Victoria 3052, Australia. [2]Institute for Molecular Bioscience, The University of Queensland, St Lucia, Queensland 4072, Australia. [3]Australian Institute for Bioengineering and Nanotechnology, The University of Queensland, St Lucia, Queensland 4072, Australia. [4]Department of Anatomy and Embryology, Leiden University Medical Center, Einthovenweg 20, 2333 ZC Leiden, The Netherlands. [5]Department of Paediatrics, The University of Melbourne, Parkville, Victoria 3010, Australia.

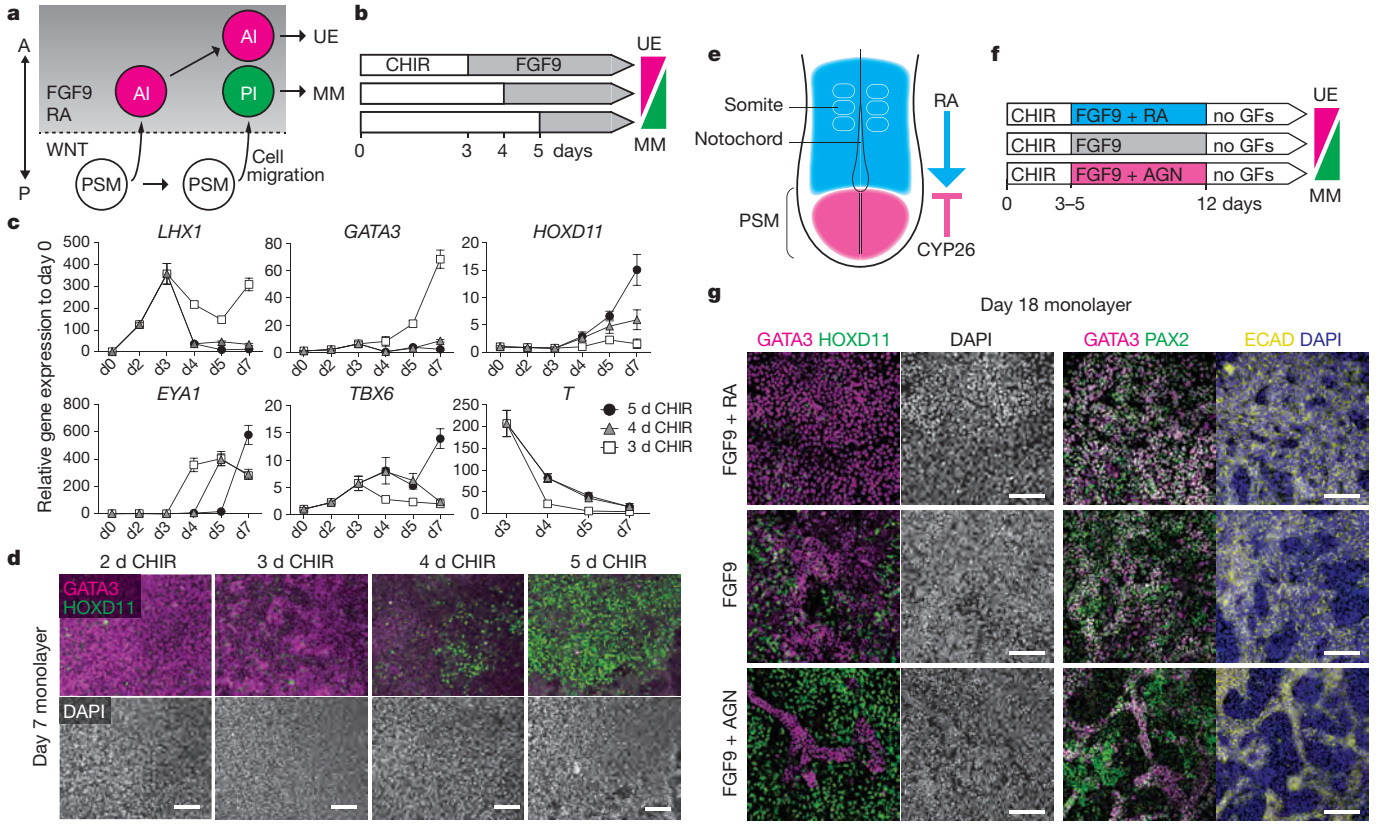

Figure 1 | Selective induction of either the collecting duct or kidney mesenchyme lineage. **a**, Schematic illustrating the mechanism of anterior–posterior (A–P) patterning of the intermediate mesoderm in the embryogenesis[13]. The timing of PSM cell migration determines the timing of the exposure to FGF9 and RA, resulting in fate selection between anterior intermediate mesoderm and posterior intermediate mesoderm. AI, anterior intermediate mesoderm; MM, metanephric mesenchyme; PI, posterior intermediate mesoderm; PSM, presomitic mesoderm; UE, ureteric epithelium. **b**, Schematic of three experimental timelines. CHIR, CHIR99021. **c**, Time course quantitative PCR of an initial 7 days (d) of the differentiation from the above timings. Experiments were conducted using monolayer culture condition (mean ± s.d., $n = 3$ independent experiments). **d**, Immunofluorescence at day 7 of differentiation with the AI marker, GATA3, and the PI marker, HOXD11. Scale bars, 100 μm. Experimental replicates, 3. **e**, Schematic illustrating RA signalling after the primitive streak stage. An RA-metabolizing enzyme, CYP26, is expressed in the PSM region to shield PSM cells from RA signalling. **f**, Schematic of three experimental timelines. RA or AGN193109 (AGN) were added with FGF9 after CHIR99021, followed by growth factor withdrawal (no GFs). Experiments were conducted with monolayer culture condition. **g**, Immunofluorescence at day 18 of differentiation from 3 days of CHIR99021 followed by ± RA/AGN. AGN inhibited the AI specification of early migrating cells, causing posteriorization. At day 18, GATA3 and HOXD11 mark the UE and the MM, respectively (left panels). $GATA3^+PAX2^+ECAD^+$ cells represent the UE whereas $GATA3^-PAX2^+$ cells do the MM ($ECAD^-$) and its derivatives ($ECAD^+$) (right panels). Experimental replicates, 3. Scale bars, 100 μm.

for nephrogenesis, suggesting an additional role for FGF signalling after Wnt-mediated nephron induction (Extended Data Fig. 3b). Within each organoid, the nephrons appropriately segmented into 4 components, including the collecting duct ($GATA3^+ECAD^+$), the early distal tubule ($GATA3^-LTL^-ECAD^+$), early proximal tubule (LTL^+ECAD^-) and the glomerulus ($WT1^+$) (Fig. 2c, d). Moreover, kidney organoids showed complex morphogenetic patterning with collecting duct trees forming at the bottom of the organoid, connecting to distal and proximal tubules in the middle, with the glomeruli at the top of each organoid (Fig. 2e and Supplementary Videos 1 and 2). This patterning mimics the tissue organization observed *in vivo* where glomeruli arise in the cortex whereas the collecting ducts radiate through the organ from the middle. Here again, the relative level of collecting duct versus nephron within individual organoids could be varied with the timing of the initial CHIR99021-to-FGF9 switch (Extended Data Fig. 4a, b). Next, we performed RNA sequencing of whole kidney organoids at day 0, 3, 11 and 18 after aggregation and 3D culture. Across this time course we observed a temporal loss of nephron progenitor gene expression but an increase in markers of multiple nephron segments, including the podocytes, proximal and distal tubules (Extended Data Fig. 5 and Supplementary Table 2). Transcriptional profiling was performed and compared using an unbiased method with human fetal transcriptional data sets from 21 human fetal organs/tissues from the first and/or second trimester of pregnancy[15]. This analysis clustered kidney organoids at d11 and d18 of culture with first trimester human fetal kidney (Fig. 2f, g and Extended Data Fig. 6). At the earlier culture time points (day 0 and 3), organoids more closely matched the fetal gonad, an embryologically closely related tissue also derived from the intermediate mesoderm.

In a kidney, the epithelial cell types (nephron and collecting duct) are surrounded by a renal interstitium (stroma) within which there is a vascular network. As well as forming the metanephric mesenchyme, the intermediate mesoderm gives rise to stromal and vascular progenitors (Fig. 3a)[16,17]. We examined kidney organoids for evidence of additional cell types and evidence of functional maturation. Collecting ducts could be distinguished based on co-expression of PAX2, GATA3 and ECAD (Fig. 3b). At d11, nephron epithelia showed proximal (LTL^+ECAD^-) and distal (LTL^-ECAD^+) elements (Fig. 3c). By day 18, proximal tubules matured to co-express LTL with ECAD, with cubilin evident on the apical surface (Fig. 3d, e). Transmission electron microscopy (TEM) showed distinct epithelial subtypes; cells with few short microvilli surrounding an open lumen characteristic of collecting duct/distal tubule (Fig. 3k) and typical proximal tubular epithelium displaying an apical brush border with tight junctions (Fig. 3l). By day 18, loops of Henle ($UMOD^+$) began to form (Fig. 3f). By day 11, $WT1^+NPHS1^+$ early glomeruli[18] comprising a Bowman's capsule

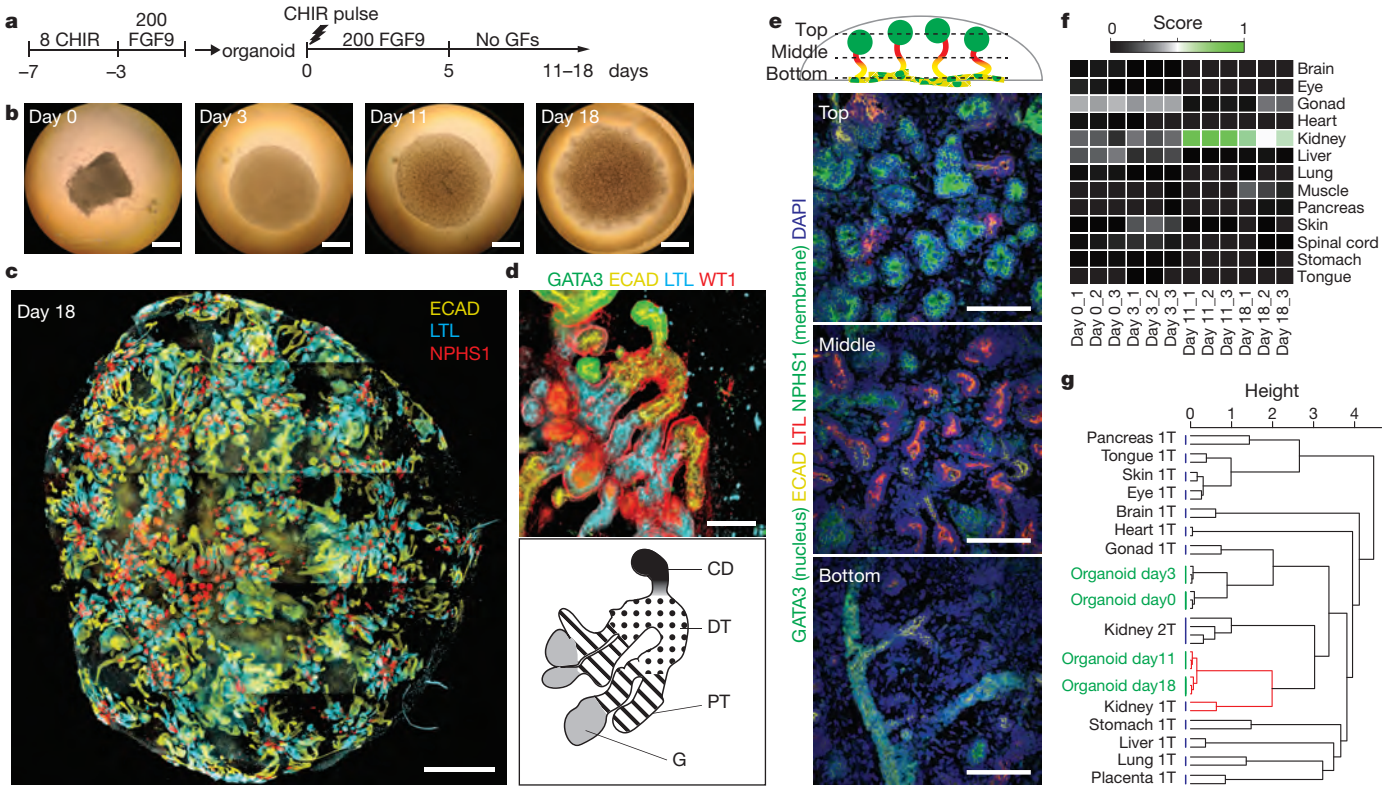

Figure 2 | Generating a kidney organoid equivalent to the human fetal kidney *in vitro*. **a**, Schematic of the differentiation protocol from hPSCs. 8 CHIR, 8 μM CHIR99021; 200 FGF9, 200 ng ml^{-1} FGF9. **b**, Global bright field observations of self-organizing kidney organoids across a time series. The success rate of organoid differentiation was 94.2% (138 organoids, 5 experiments). Scale bars, 1 mm. **c**, Tile scan immunofluorescence of a whole kidney organoid displaying structural complexity. Scale bar, 1 mm. **d**, High-power immunofluorescence microscopy showing a nephron segmented into 4 compartments, including the collecting duct (CD, GATA3$^+$ECAD$^+$), distal tubule (DT, GATA3$^-$ECAD$^+$LTL$^-$), proximal tubule (PT, ECAD$^-$LTL$^+$) and the glomerulus (G, WT1$^+$). Scale bar, 100 μm. **e**, Confocal microscopy generating serial *z*-stack images from the bottom to the top of a day 11 kidney organoid (Supplementary Videos 1 and 2). Schematic illustrates the position of different structures within an organoid. Top, middle and bottom images are representative images taken through the organoids at the position indicated in **e**. Each segment of the nephron is marked (or coloured in schematic) as described below: collecting ducts, GATA3$^+$ECAD$^+$ (green dots in yellow); distal tubules, ECAD$^+$ (yellow); proximal tubules, LTL$^+$ (red); glomeruli, NPHS1 (green circles). Scale bars, 100 μm. **f**, Heat map visualizing the relative transcriptional identity (score from 0 to 1 determined using the KeyGene algorithm[15]) of kidney organoids to 13 human fetal tissues. RNA-seq was performed on whole kidney organoids from 4 time points (day 0, 3, 11 and 18 after aggregation) with 3 individual organoids from 1 experiment per time point (see Supplementary Table 2). **g**, A dendrogram showing the hierarchical clustering of day 0, 3, 11 and 18 kidney organoids with human fetal organs from both first trimester and second trimester, based on 85 key genes (Supplementary Table 3) previously defined[15]. This clearly shows a close match with trimester 1 fetal kidney from day 11 and 18 of culture.

with central podocyte formation was seen connected to proximal tubules (Fig. 3g). Kidney organoids also developed a CD31$^+$ KDR$^+$SOX17$^+$ endothelial network with lumen formation (Fig. 3h and Extended Data Fig. 7a, b, c). TEM showed the presence of primary and secondary foot processes characteristic of podocytes (Fig. 3m). In a developing kidney, renal interstitium differentiates into pericytes and mesangial cells[19]. As expected, kidney organoids contained PDGFRA$^+$ perivascular cells that lie along KDR$^+$ endothelia and PDGFRA$^+$ early mesangial cells invaginating the glomeruli, as observed in human fetal kidney[20] (Extended Data Fig. 8a, b). Early avascular glomeruli contained basement membrane, as indicated by laminin staining and TEM, and showed attaching foot processes on the basement membrane (Extended Data Fig. 8c, d). In some instances, glomeruli showed evidence of endothelial invasion (Fig. 3i and Supplementary Videos 3 and 4), a feature never observed in explanted embryonic mouse kidneys[21]. Finally, nephrons were surrounded by MEIS1$^+$ renal interstitial cells[22], some of which were also FOXD1$^+$ (Fig. 3j and Extended Data Fig. 8e), suggesting the presence of cortical (FOXD1$^+$MEIS1$^+$) and medullary (FOXD1$^-$MEIS1$^+$) stroma. Hence, all anticipated kidney components form, pattern and begin to mature within these hPSC-derived kidney organoids. Consistent with these observations were the transcriptional changes across time in culture, with a gradual reduction in the nephrogenic mesenchyme and ureteric tip markers followed by the upregulation of genes specific to podocyte, proximal tubule, distal tubule and loop of Henle[23].(Extended Data Fig. 5).

The utility of stem-cell derived kidney organoids for disease modelling or drug screening will be dependent upon the functional maturation of the nephrons within these organoids. To test this, we focused on the proximal tubules, a nephron segment that has important roles in solute, vitamin, hormone and amino acids reabsorption. The capacity of cubilin-mediated proximal tubule specific endocytosis was demonstrated by the selective uptake of dextran–Alexa488 from the media by the LTL$^+$ tubules after 24 h of exposure (Fig. 4a and Extended Data Fig. 9a, b). The proximal tubules represent a particular target for nephrotoxicity due to the expression of multidrug resistance (such as ABCB1, ABCG2) and anion and cation transporters (such as the SLC22 gene family)[24]. Cisplatin is one such nephrotoxicant that induces caspase-mediated acute apoptosis of proximal tubular cells in the kidney[25,26]. We treated kidney organoids with 0, 5 and 20 μM cisplatin for 24 h before examining cleaved-CASP3 antibody staining (Extended Data Fig. 9c). While control organoids showed occasional apoptotic interstitial cells, both 5 μM and 20 μM cisplatin induced specific acute apoptosis in mature proximal tubular cells (LTL$^+$ECAD$^+$), whereas immature cells (LTL$^+$ECAD$^-$) did not undergo apoptosis (Fig. 4b, c).

In summary, this study demonstrates that by carefully balancing anterior–posterior patterning of intermediate mesoderm with small

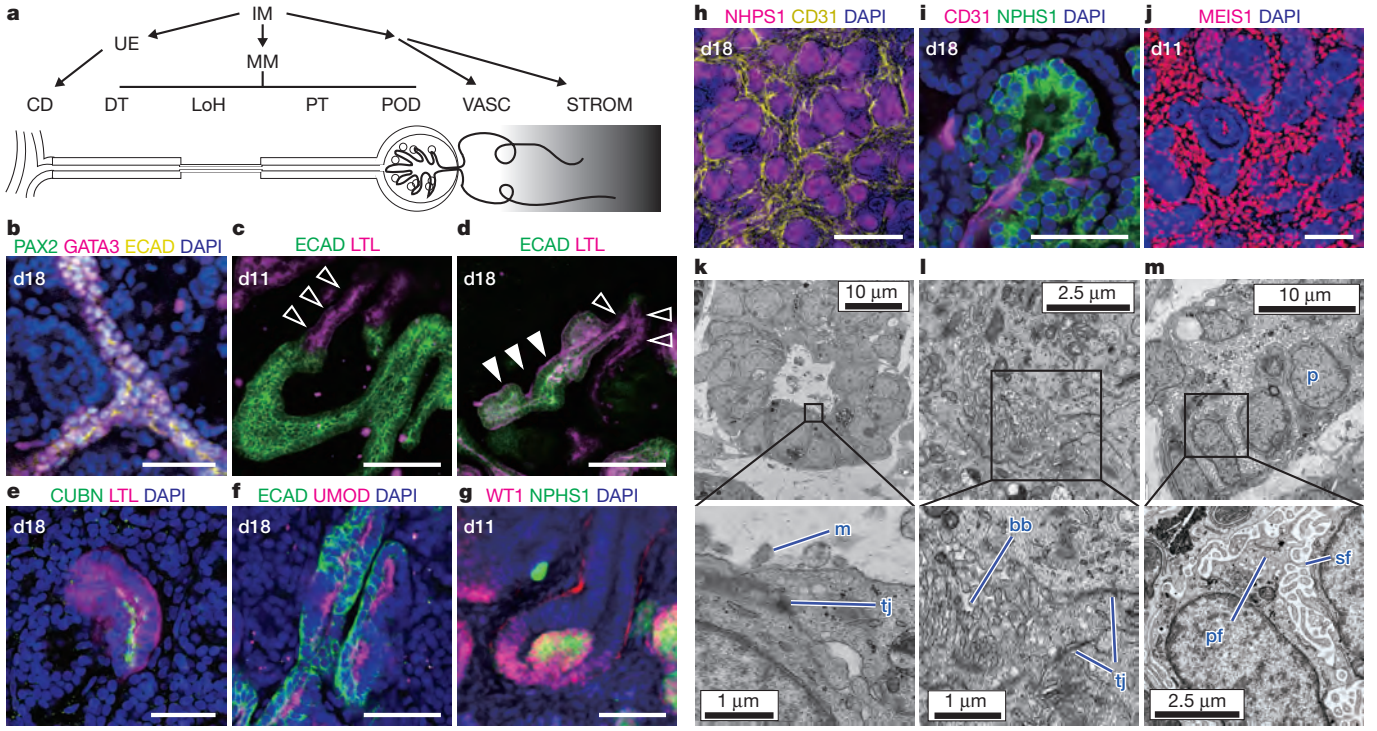

Figure 3 | Kidney organoids contain differentiating nephrons, stroma and vasculature with progressive maturation with time in culture. **a**, Schematic illustrating the developmental pathway from intermediate mesoderm (IM) to each cellular component of the kidney. CD, collecting ducts; DT, distal tubules; LoH, loops of Henle; PT, proximal tubules; POD, podocytes; VASC, vasculature; STROM, renal interstitium. **b**–**j**, Immunofluorescence of kidney organoids at either day 11 or 18. **b**, Collecting ducts marked by PAX2, GATA3 and ECAD. Scale bar, 50 µm. **c**, **d**, Early proximal tubules of LTL^+ECAD^- at day 11 (black arrowheads). LTL^+ECAD^+ maturing proximal tubules appear by day 18 (white arrowheads). Scale bars, 100 µm. **e**, Proximal tubules express cubilin (CUBN). Scale bar, 50 µm. **f**, Loops of Henle marked by UMOD and ECAD. Scale bar, 50 µm. **g**, A developing glomerulus with podocytes marked by WT1 and NPHS1. Scale bar, 50 µm. **h**, $CD31^+$ endothelia within the renal interstitium. Scale bar, 200 µm. **i**, Evidence of endothelial invasion into glomeruli at day 18 of culture. Scale bar, 50 µm. **j**, The kidney interstitium marked by MEIS1. Scale bar, 100 µm. **k**–**m**, Transmission electron microscopy of kidney organoids. **k**, A putative distal tubule with relatively sparse short microvilli (m) and tight junctions (tj). **l**, A putative proximal tubule with a lumen filled with extensive closely packed microvilli characteristic of the brush border (bb). **m**, Podocytes (p) with characteristic large nuclei and primary (pf) and secondary foot (sf) processes. Data are representative from a minimum of 3 independent experiments.

molecules it is possible to direct human pluripotent stem cells to form a complex multicellular kidney organoid that comprises fully segmented nephrons surrounded by endothelia and renal interstitium and is transcriptionally similar to a human fetal kidney. As such, these will improve our understanding of human kidney development. Each kidney organoid reaches a substantial size with more than 500 nephrons per organoid, a number equivalent to a mouse kidney at 14.5 days post-coitum[27]. While there is room for further improvement with regard to

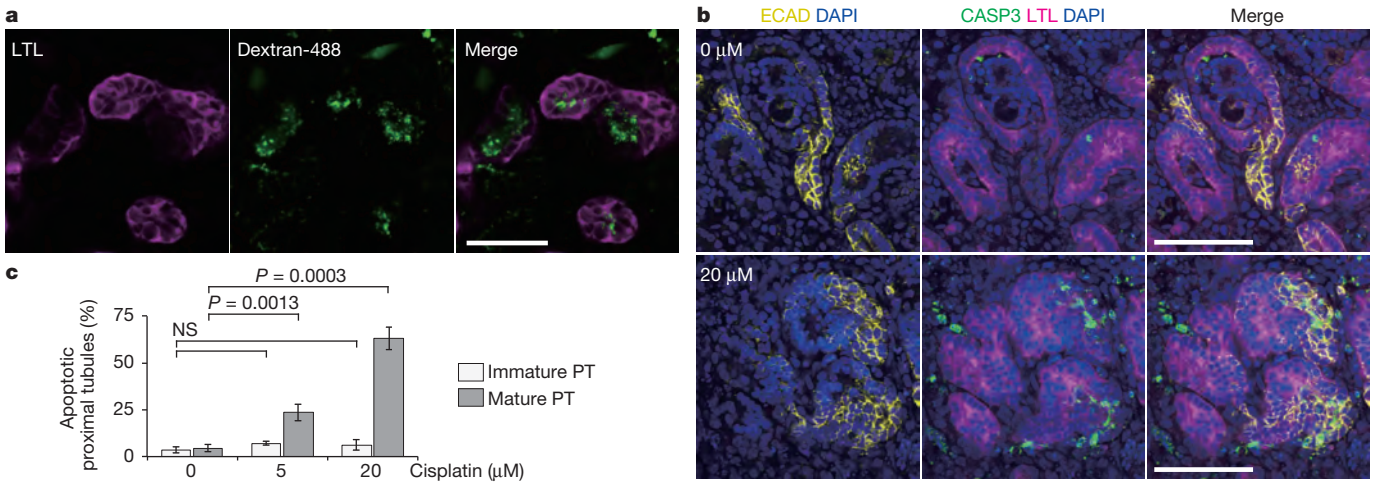

Figure 4 | Functional maturation of the proximal tubule. **a**, Dextran uptake assay showing endocytic ability of LTL^+ tubules. Scale bar, 50 µm. **b**, Treating kidney organoids with 20 µM cisplatin caused apoptosis in LTL^+ECAD^+ proximal tubular cells. Apoptotic cells were detected by cleaved caspase 3 antibody-staining (CASP3). Scale bars, 100 µm. **c**, Quantification of the number of apoptotic tubules showing mature proximal tubules-specific apoptosis by a nephrotoxicant, cisplatin. In response to 5 µM and 20 µM cisplatin, LTL^+ECAD^+ mature proximal tubules (PT) underwent apoptosis dose-dependently. In contrast, LTL^+ECAD^- immature PT did not respond to cisplatin. *P* values were calculated by independent *t*-test (mean ± s.e.m., $n = 5$ independent experiments); NS, not significant.

tubular functional maturity, glomerular vascularisation and a contiguous collecting duct epithelium with a single exit path for urine, the tissue complexity and degree of organoid functionalization observed here supports their use to screen drugs for toxicity, modelling genetic kidney disease or act as a source of specific kidney cell types for cellular therapy.

Online Content Methods, along with any additional Extended Data display items and Source Data, are available in the online version of the paper; references unique to these sections appear only in the online paper.

Received 18 June; accepted 8 September 2015.
Published online 7 October 2015.

1. Takasato, M. *et al.* Directing human embryonic stem cell differentiation towards a renal lineage generates a self-organizing kidney. *Nature Cell Biol.* **16,** 118–126 (2014).
2. James, R. G. & Schultheiss, T. M. Patterning of the avian intermediate mesoderm by lateral plate and axial tissues. *Dev. Biol.* **253,** 109–124 (2003).
3. Mae, S. *et al.* Monitoring and robust induction of nephrogenic intermediate mesoderm from human pluripotent stem cells. *Nat. Commun.* **4,** 1367 (2013).
4. Xia, Y. *et al.* Directed differentiation of human pluripotent cells to ureteric bud kidney progenitor-like cells. *Nature Cell Biol.* **15,** 1507–1515 (2013).
5. Taguchi, A. *et al.* Redefining the *in vivo* origin of metanephric nephron progenitors enables generation of complex kidney structures from pluripotent stem cells. *Cell Stem Cell* **14,** 53–67 (2014).
6. Lam, A. Q. *et al.* Rapid and efficient differentiation of human pluripotent stem cells into intermediate mesoderm that forms tubules expressing kidney proximal tubular markers. *J. Am. Soc. Nephrol.* **25,** 1211–1225 (2014).
7. Kang, M. & Han, Y. M. Differentiation of human pluripotent stem cells into nephron progenitor cells in a serum and feeder free system. *PLoS One* **9,** e94888 (2014).
8. Xu, J. *et al.* Eya1 interacts with Six2 and Myc to regulate expansion of the nephron progenitor pool during nephrogenesis. *Dev. Cell* **31,** 434–447 (2014).
9. Duester, G. Retinoic acid synthesis and signaling during early organogenesis. *Cell* **134,** 921–931 (2008).
10. Sakai, Y. *et al.* The retinoic acid-inactivating enzyme CYP26 is essential for establishing an uneven distribution of retinoic acid along the anterio-posterior axis within the mouse embryo. *Genes Dev.* **15,** 213–225 (2001).
11. Abu-Abed, S. *et al.* The retinoic acid-metabolizing enzyme, CYP26A1, is essential for normal hindbrain patterning, vertebral identity, and development of posterior structures. *Genes Dev.* **15,** 226–240 (2001).
12. Sweetman, D., Wagstaff, L., Cooper, O., Weijer, C. & Münsterberg, A. The migration of paraxial and lateral plate mesoderm cells emerging from the late primitive streak is controlled by different Wnt signals. *BMC Dev. Biol.* **8,** 63 (2008).
13. Takasato, M. & Little, M. H. The origin of the mammalian kidney: implications for recreating the kidney *in vitro*. *Development* **142,** 1937–1947 (2015).
14. Park, J. S. *et al.* Six2 and Wnt regulate self-renewal and commitment of nephron progenitors through shared gene regulatory networks. *Dev. Cell* **23,** 637–651 (2012).
15. Roost, M. S. *et al.* KeyGenes, a tool to probe tissue differentiation using a human fetal transcriptional atlas. *Stem Cell Reports* **4,** 1112–1124 (2015).
16. Mugford, J. W., Sipilä, P., McMahon, J. A. & McMahon, A. P. Osr1 expression demarcates a multi-potent population of intermediate mesoderm that undergoes progressive restriction to an Osr1-dependent nephron progenitor compartment within the mammalian kidney. *Dev. Biol.* **324,** 88–98 (2008).
17. Sims-Lucas, S. *et al.* Endothelial progenitors exist within the kidney and lung mesenchyme. *PLoS One* **8,** e65993 (2013).
18. Brunskill, E. W., Georgas, K., Rumballe, B., Little, M. H. & Potter, S. S. Defining the molecular character of the developing and adult kidney podocyte. *PLoS One* **6,** e24640 (2011).
19. Kobayashi, A. *et al.* Identification of a multipotent self-renewing stromal progenitor population during mammalian kidney organogenesis. *Stem Cell Reports* **3,** 650–662 (2014).
20. Floege, J. *et al.* Localization of PDGF alpha-receptor in the developing and mature human kidney. *Kidney Int.* **51,** 1140–1150 (1997).
21. Loughna, S., Yuan, H. T. & Woolf, A. S. Effects of oxygen on vascular patterning in Tie1/LacZ metanephric kidneys *in vitro*. *Biochem. Biophys. Res. Commun.* **247,** 361–366 (1998).
22. Brunskill, E. W. *et al.* Atlas of gene expression in the developing kidney at microanatomic resolution. *Dev. Cell* **15,** 781–791 (2008).
23. Thiagarajan, R. D. *et al.* Identification of anchor genes during kidney development defines ontological relationships, molecular subcompartments and regulatory pathways. *PLoS One* **6,** e17286 (2011).
24. Cheng, X. & Klaassen, C. D. Tissue distribution, ontogeny, and hormonal regulation of xenobiotic transporters in mouse kidneys. *Drug Metab. Dispos.* **37,** 2178–2185 (2009).
25. Mese, H., Sasaki, A., Nakayama, S., Alcalde, R. E. & Matsumura, T. The role of caspase family protease, caspase-3 on cisplatin-induced apoptosis in cisplatin-resistant A431 cell line. *Cancer Chemother. Pharmacol.* **46,** 241–245 (2000).
26. Cummings, B. S. & Schnellmann, R. G. Cisplatin-induced renal cell apoptosis: caspase 3-dependent and -independent pathways. *J. Pharmacol. Exp. Ther.* **302,** 8–17 (2002).
27. Short, K. M. *et al.* Global quantification of tissue dynamics in the developing mouse kidney. *Dev. Cell* **29,** 188–202 (2014).

Supplementary Information is available in the online version of the paper.

Acknowledgements This research was supported by National Health and Medical Research Council (NHMRC) of Australia (APP1041277, APP1037320), Australian Research Council (ARC) (SRI110001002, CE140100036), Bontius Stiching and Organovo Inc. M.H.L. and R.G.P. are NHMRC Senior Principal Research Fellows. B.M. is a Rosamond Siemon Postgraduate Scholar. We thank A. Christ and T. Bruxner at the IMB Sequencing Facility for providing NGS service. We also acknowledge the IMB ACRF Imaging Facility and the Australian Microscopy & Microanalysis Research Facility at the Center for Microscopy and Microanalysis at The University of Queensland.

Author Contributions M.T. and M.H.L. planned the project, designed experiments, analysed and interpreted data and wrote the manuscript. M.T. performed experiments. P.X.E. maintained hES/iPS cells. P.X.E. and H.S.C. performed experiments under the supervision of M.T and M.H.L.; B.M. generated organoids for TEM. G.J.B. analysed bioinformatic data. C.F. performed TEM. R.G.P. captured and interpreted TEM images. E.J.W. provided the iPS cell line and advised on general iPS cell quality control. M.S.R. and S.M.C.d.S.L. developed NGS analytical tools and analysed data for RNA-seq profiling.

Author Information The RNA-seq data have been deposited in the Gene Expression Omnibus (http://www.ncbi.nlm.nih.gov/geo/) under accession number GSE70101. Reprints and permissions information is available at www.nature.com/reprints. The authors declare competing financial interests: details are available in the online version of the paper. Readers are welcome to comment on the online version of the paper. Correspondence and requests for materials should be addressed to M.T. (minoru.takasato@mcri.edu.au) or M.H.L. (melissa.little@mcri.edu.au).

METHODS

No statistical methods were used to predetermine sample size, the experiments were not randomized and the investigators were not blinded to allocation during experiments and outcome assessment.

Cell culture and differentiation. All experiments presented used the previously described wild-type human iPS cell line CRL1502 (clone C32) generated using episomal reprogramming[28]. Undifferentiated human iPS cells were maintained on the mouse embryonic fibroblasts (MEFs) (Millipore) as a feeder layer with human ES cell (hES) medium as described previously[1]. Cells were authenticated and tested for the mycoplasma infection[28]. Human iPS cells were plated on a Matrigel-coated (Millipore) culture dish and cultured in MEF-conditioned hES medium (MEF-CM) until reaching 60–100% confluence. Then, cells were again plated on a Matrigel-coated at 5,000 cells per cm^2 in MEF-CM. Next day, cells reached 40–50% of confluence, cells were treated with 8 μM CHIR99021 in APEL basal medium (STEMCELL Technologies) supplemented with Antibiotic-Antimycotic (Life Technologies) for 2–5 days, followed by FGF9 (200 ng ml^{-1}) and heparin (1 μg ml^{-1}) for another 5–2 days, with changing medium every second day. At day 7, cells were collected and dissociated into single cells using trypsin or TrypLE select (Life Technologies). Cells (0.5×10^6) were spun down at ×400*g* for 2 min to form a pellet and then transferred onto a Transwell 0.4 μm pore polyester membrane (CLS3450 Corning). Pellets were treated with 5 μM CHIR99021 in APEL for 1 h, and then cultured with FGF9 (200 ng ml^{-1}) and heparin (1 μg ml^{-1}) for 5 days, followed by another 6–13 days in APEL basal medium, with changing medium three times a week. Culture medium should not overflow over the membrane. For the differentiation in monolayer cultures, cells after CHIR99021 induction were treated by FGF9 (200 ng ml^{-1}) and heparin (1 μg ml^{-1}) for 10 days, followed by APEL basal medium for another 6 days. In some experiments, RA (0.1 μM) or AGN193109 (5 μM) were added to FGF9 medium. A step-by step protocol describing kidney organoid generation can be found at Protocol Exchange[29].

Immunocytochemistry. For monolayer cells, antibody staining was performed as described previously[1]. For the kidney organoid, organoids were fixed with 2% paraformaldehyde in PBS for 20 min at 4 °C followed by 3 times wash with PBS. Then organoids were blocked with 10% donkey serum, 0.3% Triton X/PBS for 2–3 h at room temperature and incubated with primary antibodies overnight at 4 °C. After 5 times washing with 0.1% Triton X/PBS, secondary antibodies were incubated for 4 h at room temperature. The following antibodies and dilutions were used: rabbit anti-PAX2 (1:300, 71-6,000, Zymed Laboratories), goat anti-SIX1 (1:300, sc-9709, Santa Cruz Biotechnology), rabbit anti-SIX2 (1:300, 11562-1-AP, Proteintech), mouse anti-ECAD (1:300, 610181, BD Biosciences), rabbit anti-WT1 (1:100, sc-192, Santa Cruz Biotechnology), mouse anti-HOXD11 (1:300, SAB1403944, Sigma-Aldrich), goat anti-GATA3 (1:300, AF2605, R&D Systems), rabbit anti-JAG1 (1:300, ab7771, Abcam), goat anti-cubilin (1:150, sc-20607, Santa Cruz Biotechnology), sheep anti-NPHS1 (1:300, AF4269, R&D Systems), LTL-biotin-conjugated (1:300, B-1325, Vector Laboratories), DBA-biotin-conjugated (1:300, B-1035, Vector Laboratories), mouse anti-KRT8 (1:300, TROMA, DSHB), mouse anti-CD31 (1:300, 555444, BD Pharmingen), rabbit anti-KDR (1:300, 2479, Cell Signaling Technology), goat anti-SOX17 (1:300, AF1924, R&D Systems), mouse anti-PDGFRA (1:200, 556001, BD Pharmingen), rabbit anti-Laminin (1:300, L9393, Sigma-Aldrich), rabbit anti-UMOD (1:300, BT-590, Biomedical Technologies), mouse anti-MEIS1 (1:300, ATM39795, activemotif), goat anti-FOXD1 (1:200, sc-47585, Santa Cruz Biotechnology) and rabbit anti-cleaved-CASP3 (1:300, 9661, Cell Signaling Technology). Images were taken using a Nikon Ti-U microscope or a Zeiss LSM 780 confocal microscope. All immunofluorescence analyses were successfully repeated more than three times and representative images are shown.

Electron microscopy. Organoids were processed for electron microscopy using a method as follows. A solution of 5% glutaraldehyde in 2 × PBS was added directly to the organoid culture dish in equal volume to the growth medium and placed under vacuum for 5 min. The organoid was reduced in size by cutting into small blocks (~2 × 2 mm), and irradiated in fresh fixative 2.5%, again under vacuum, for 6 min, in a Pelco Biowave (Ted Pella In, Redding, CA) at 80 W power. Samples were then washed 4 × 2 min in 0.1 M cacodylate buffer. Samples were then immersed in a solution containing potassium ferricyanide (3%) and osmium tetroxide (2%) in 0.1 M cacodylate buffer for 30 min at room temperature. Following 6 × 3 min washes in distilled water the tissue blocks were then incubated in a filtered solution containing thiocarbohydrazide (1%) for 30 min at room temperature. After subsequent washing in distilled water (6 × 2 min) samples were incubated in an aqueous solution of osmium tetroxide (2%) for 30 min, then in distilled water (6 × 2 min) and incubated in 1% aqueous uranyl acetate for 30 min at 4 °C. After further distilled water washes (2 × 2 min) a freshly prepared filtered solution of 0.06% lead nitrate in aspartic acid (pH 5.5) warmed to 60 °C was added to the dish and further incubated for 20 min at 60 °C before rinsing in distilled water (6 × 3 min) at room temperature. Tissue blocks were dehydrated twice in each ethanol solution of 30%, 50%, 70%, 90% and absolute ethanol for 40 s at 250 W in the Pelco Biowave. Epon LX112 resin was used for embedding the tissue with infiltration at 25%, 50%, and 75% resin:absolute ethanol in the Pelco Biowave under vacuum at 250 W for 3 min and finishing with 100% resin (twice), before the final embedding/blocking and curing at 60 °C for 12 h.

qRT–PCR analysis. Total RNA was extracted from cells using Purelink RNA mini kit (Life Technologies) and cDNA was synthesized from >100 ng total RNA using Super Script III reverse transcriptase (Life Technologies). qRT–PCR analyses were performed with GoTaq qPCR Master Mix (Promega) by Roche LightCycler 96 real-time PCR machine. All absolute data were first normalized to GAPDH and then normalized to control samples ($\Delta\Delta C_t$ method). The sequences of primers used for qRT–PCR are as listed in Supplementary Table 1.

Next generation RNA sequencing and comparative analysis using KeyGenes. Sequencing was performed using the Illumina NextSeq500 (NextSeq control software v1.2/Real Time Analysis v2.1) platform. The library pool was diluted and denatured according to the standard NextSeq500 protocol and sequencing was carried out to generate single-end 76 bp reads using a 75 cycle NextSeq500 High Output reagent Kit (Catalog FC-404-1005). Reads were mapped against the reference human genome (hg19) using STAR[30], and read counts for each gene in the UCSC annotation were generated using htseq-count in the HTSeq python package (http://www-huber.embl.de/users/anders/HTSeq/doc/index.html). The number of uniquely mapped reads ranged from 18,810,634 to 36,706,805 per sample. Normalized read counts were calculated using the DESeq2 package[31].

KeyGenes was used to generate the identity scores of day 0, 3, 11 and 18 kidney organoids to different first trimester human organs, including the kidneys (GSE66302)[15]. The dendrogram showing the hierarchical clustering of day 0, 3, 11 and 18 kidney organoids and 21 human fetal organs from first and second trimester (GSE66302) was based on the Pearson correlation of the expression levels of 85 classifier genes as determined by KeyGenes (http://www.keygenes.nl) (Supplementary Table 3). The classifier genes were calculated by KeyGenes using the top 500 most differentially expressed genes of the human fetal data without including the extraembryonic tissues from that data set.

Functional analysis for proximal tubules. For dextran uptake assay, organoids at day 17 were cultured with 10 μg ml^{-1} of 10,000 MW dextran Alexa488-conjugated (D-22910, Life Technologies) for 24 h. Organoids were fixed and stained by LTL without permeabilization. For nephrotoxicity assays, organoids at day 17 were cultured with 0, 5, 20 or 100 μM cisplatin (Sigma-Aldrich) for 24 h. The ratio of apoptotic proximal tubules to total proximal tubules was manually counted using ImageJ in 2 or 3 representative fields per experiment. In total, $n = 5$ independent experiments. Images were taken using Zeiss LSM 780 confocal microscope.

28. Briggs, J. A. *et al.* Integration-free induced pluripotent stem cells model genetic and neural developmental features of down syndrome etiology. *Stem Cells* **31,** 467–478 (2013).
29. Takasato, M., Er, X. P., Chiu, S. H. & Little, H. M. Generation of kidney organoids from human pluripotent stem cells. *Protoc. Exch.* http://dx.doi.org/10.1038/protex.2015.087 (2015).
30. Dobin, A. *et al.* STAR: ultrafast universal RNA-seq aligner. *Bioinformatics* **29,** 15–21 (2013).
31. Love, M. I., Huber, W. & Anders, S. Moderated estimation of fold change and dispersion for RNA-seq data with DESeq2. *Genome Biol.* **15,** 550 (2014).

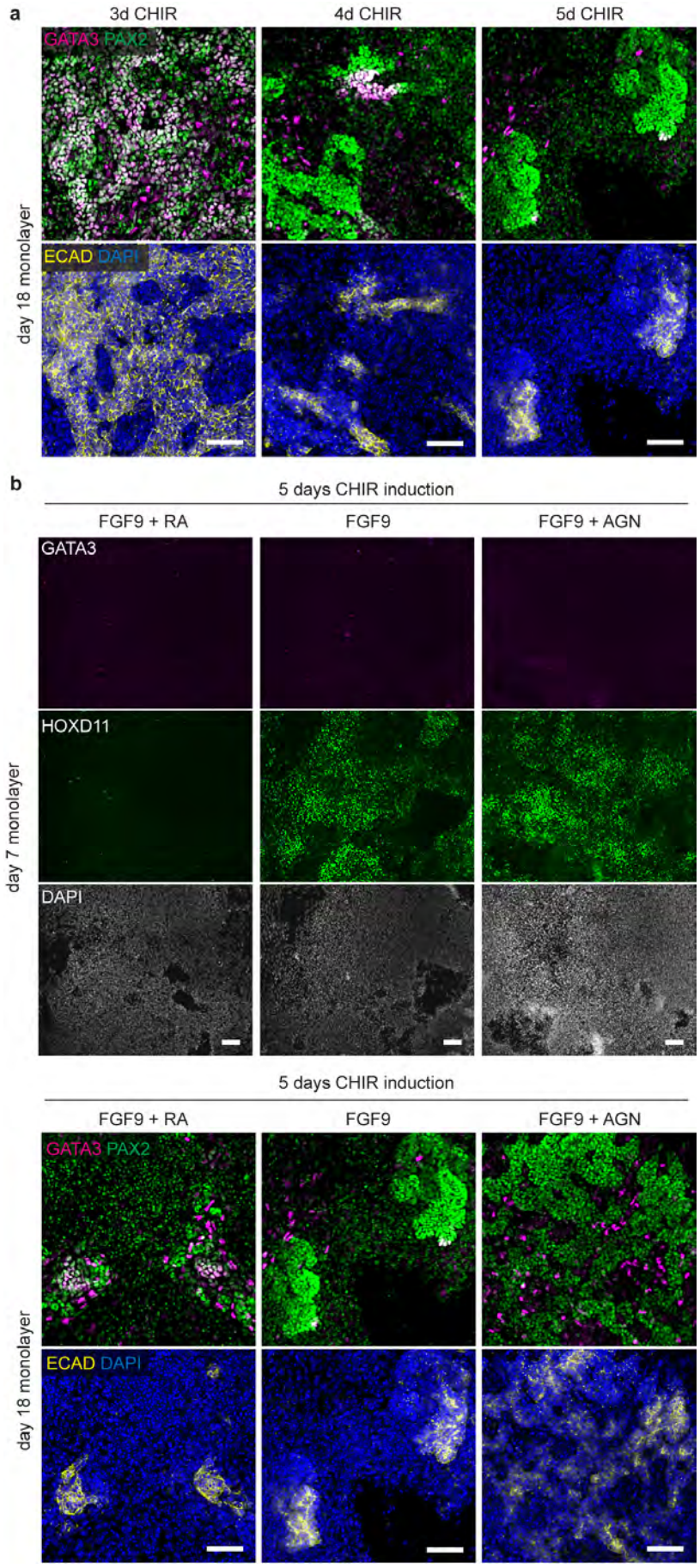

Extended Data Figure 1 | Antero-posterior intermediate mesoderm specification is regulated by the timing of FGF9 exposure and the presence of RA signalling. **a**, Immunofluorescence at day 18 of monolayer differentiation from cultures exposed to different timing of FGF9 addition (after 2, 3, 4 and 5 days of CHIR99021). The ureteric epithelium is represented by $GATA3^{+}PAX2^{+}ECAD^{+}$ cells. The metanephric mesenchyme and its derivatives are marked by $PAX2^{+}GATA3^{-}ECAD^{-}$ (metanephric mesenchyme) and $PAX2^{+}GATA3^{-}ECAD^{+}$ (nephrons), respectively. Scale bars, 100 μm. **b**, Immunofluorescence at day 7 and 18 of monolayer differentiation using 5 days of CHIR99021 followed by RA or AGN193109 (AGN) on top of FGF9. RA reduced the specification of posterior intermediate mesoderm, as indicated by the reduction of HOXD11 at day 7 (top panel). This resulted in less metanephric mesenchyme but some ureteric epithelium by RA at day 18 (bottom panel). Scale bars, 100 μm.

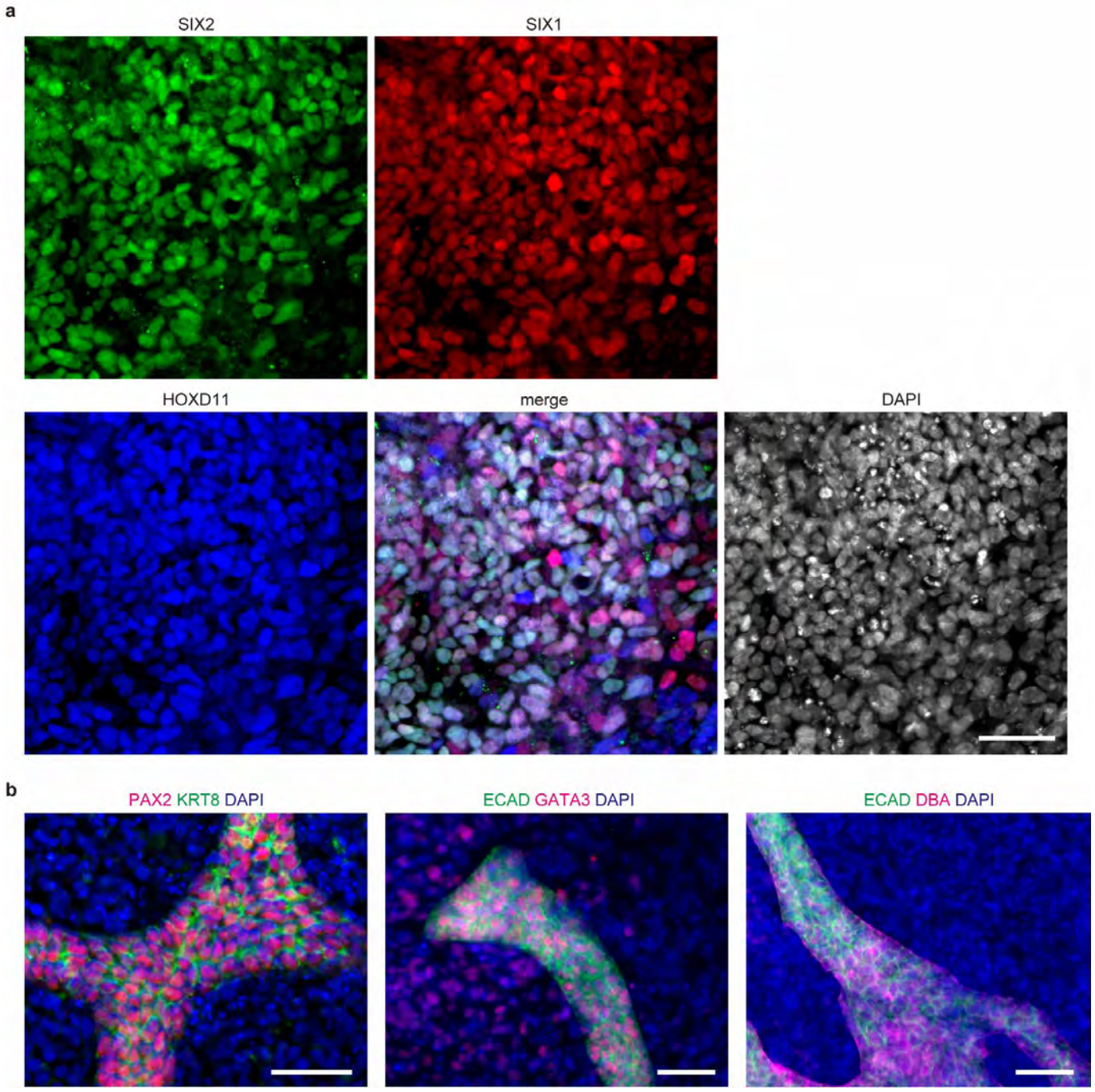

Extended Data Figure 2 | Induction of both kidney progenitors at the same time. **a**, **b**, Immunofluorescence at day 18 of the monolayer differentiation using the 4 days CHIR99021 before FGF9 protocol. The metanephric mesenchyme is marked by $SIX2^+SIX1^+HOXD11^+$ cells (**a**). $GATA3^+PAX2^+ECAD^+KRT8^+$ cells representing the ureteric epithelium were also induced (**b**). Scale bars, 50 μm.

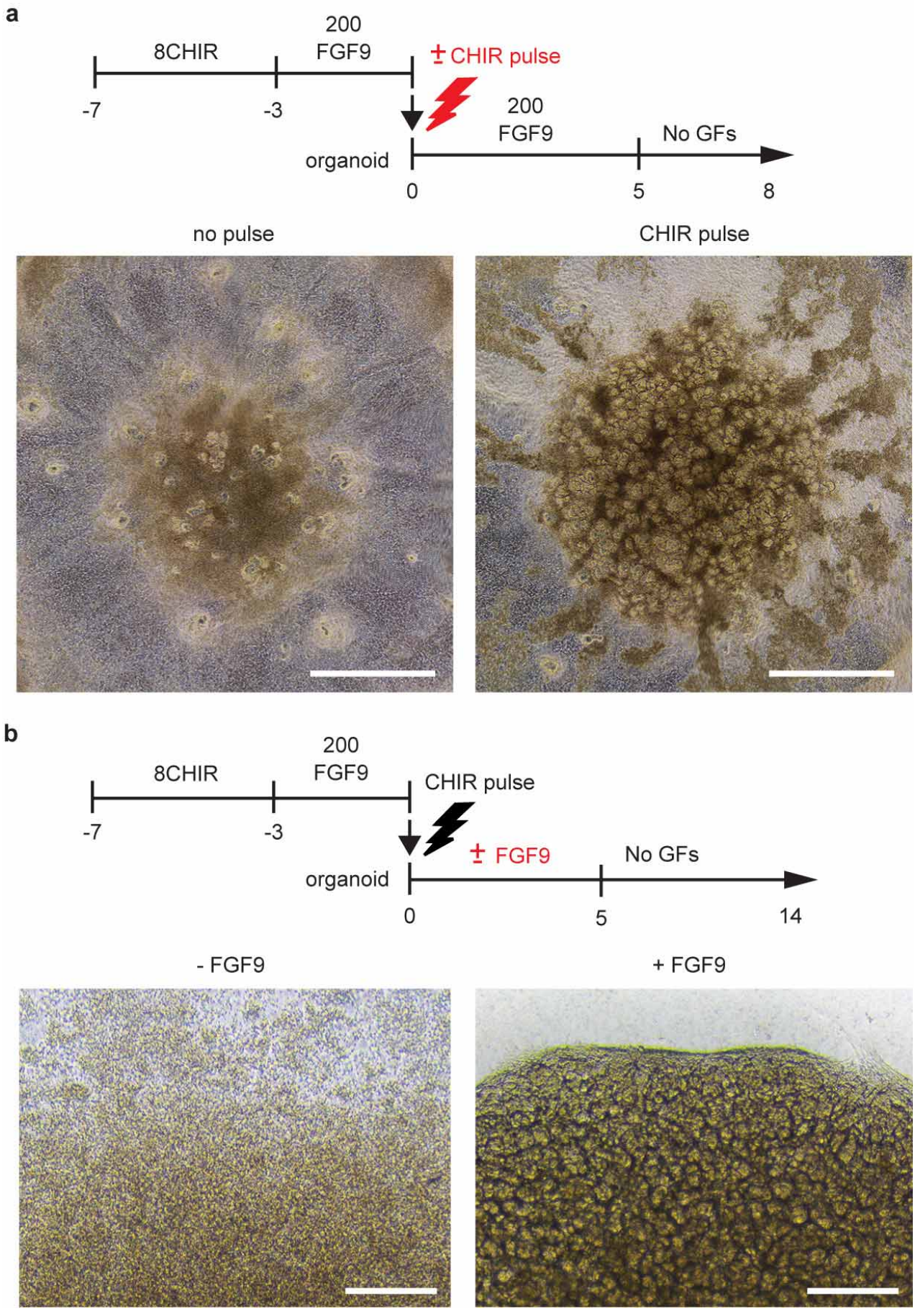

Extended Data Figure 3 | Regulation of nephrogenesis in the kidney organoid. a, Stimulating organoids with 5 μM CHIR99021 for 1 h immediately after aggregation promoted nephrogenesis (CHIR pulse), whereas only limited numbers of nephrogenesis events happened without CHIR99021 (no pulse). Scale bars, 1 mm. **b**, Without the addition of FGF9 after this CHIR99021 pulse, organoids did not initiate nephrogenesis (−FGF9). Scale bars, 200 μm.

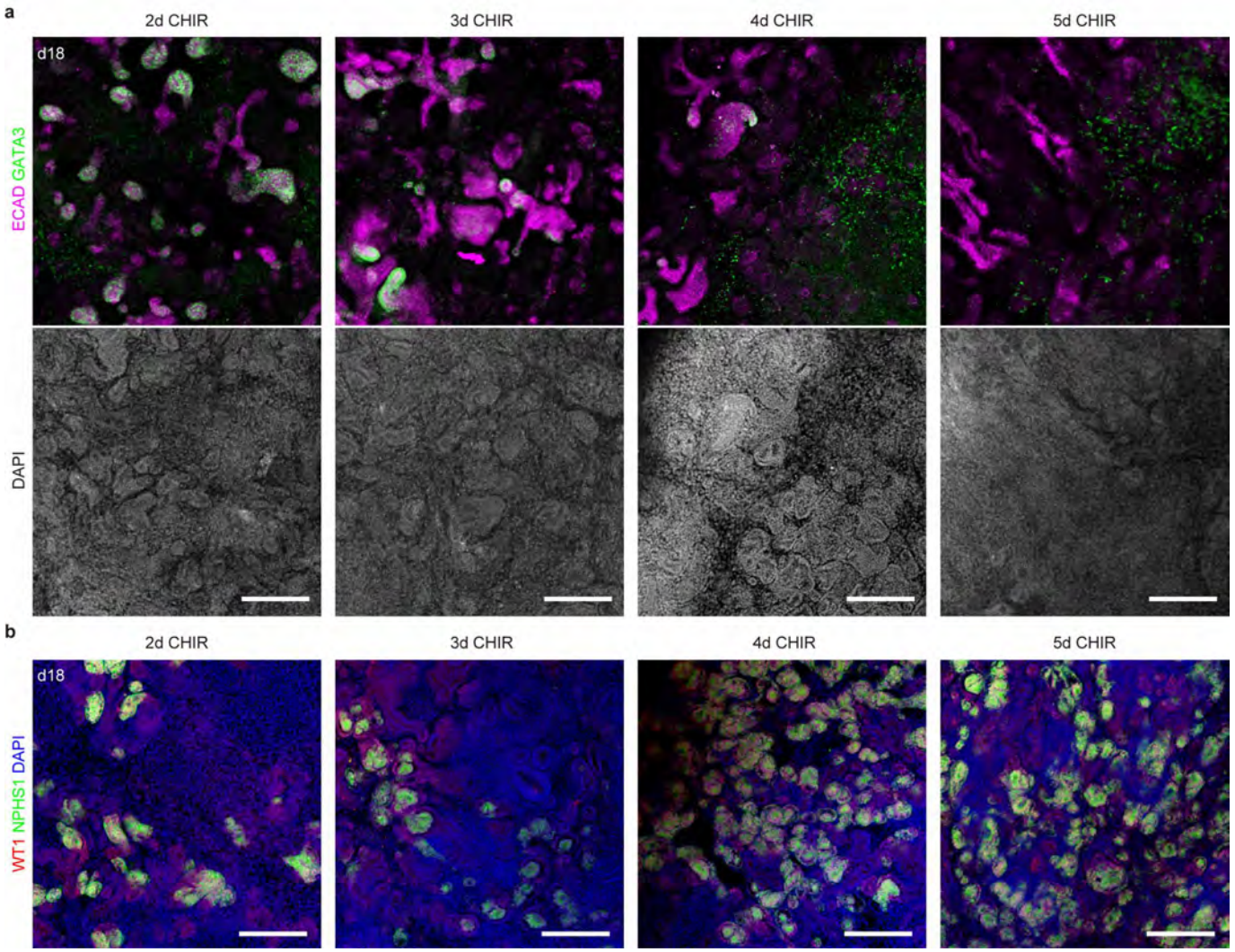

Extended Data Figure 4 | The timing of FGF9 exposure affects the ratio of collecting duct to nephron in the kidney organoid. **a**, **b**, Immunofluorescence of kidney organoids at day 18 after-aggregation after exposure to different timings of initial FGF9 exposure (2, 3, 4 and 5 days of CHIR99021 pre-FGF9), demonstrating the regulation of collecting duct/nephron ratio by varying this timing. $GATA3^{+}ECAD^{+}$ cells represent the collecting duct (**a**), whereas $WT1^{+}NPHS1^{+}$ cells mark podocytes of the glomerulus (**b**). Scale bars, 200 μm.

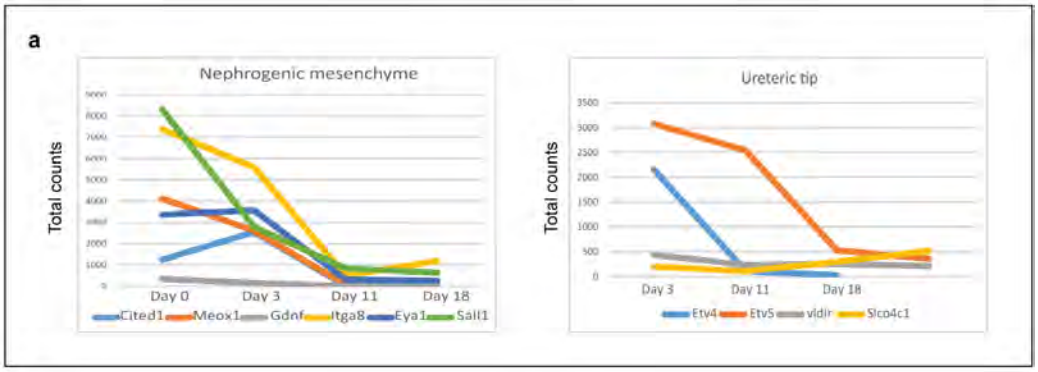

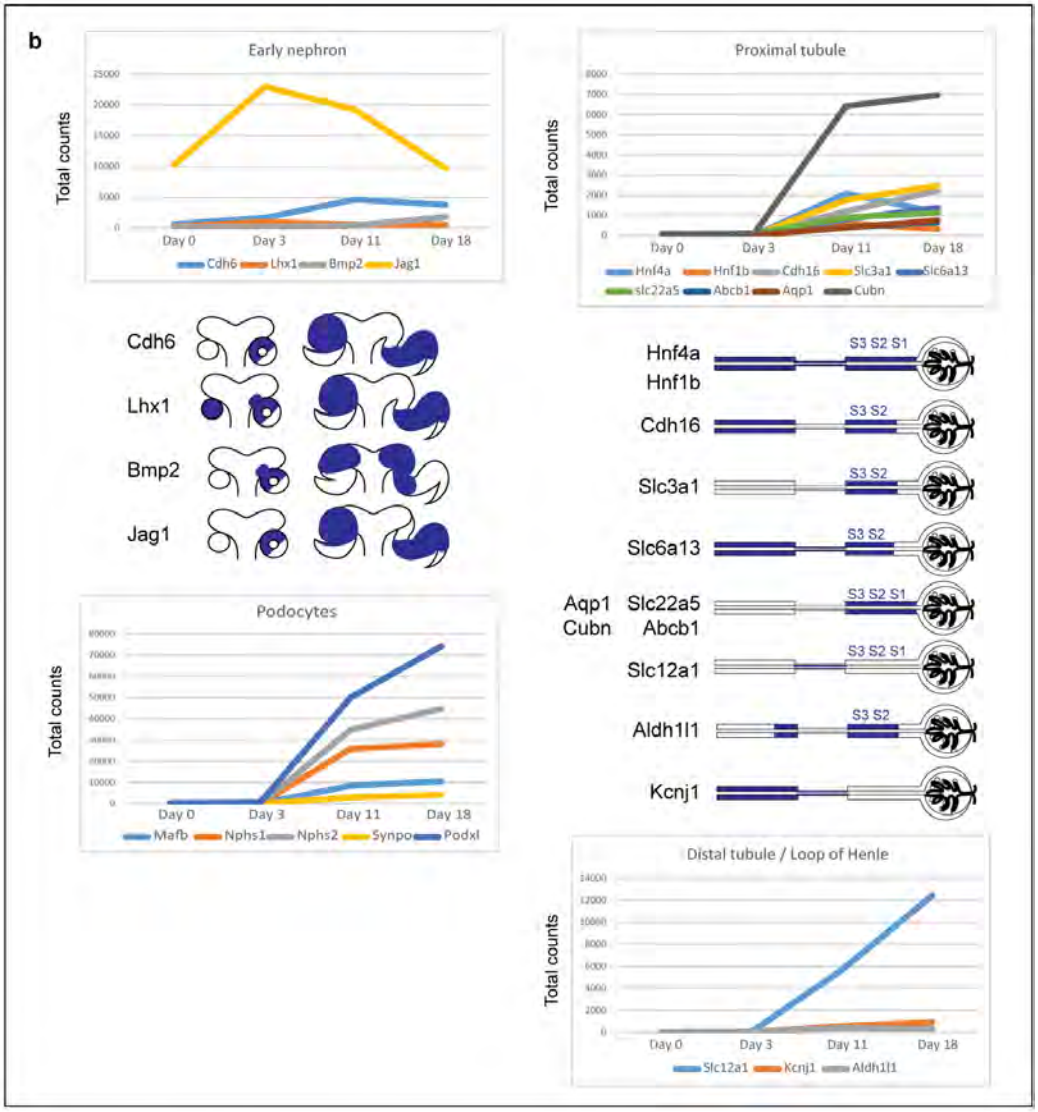

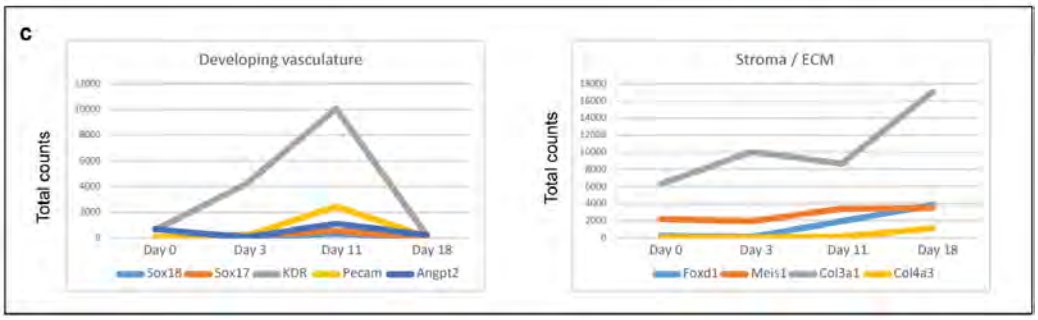

Extended Data Figure 5 | Changes of gene expression during development of the kidney organoid. **a–c**, Graphs showing expression changes of selected marker genes at 4 time points (day 0, 3, 11 and 18) of the kidney organoid culture. *y* axis represents the count of detection for each gene in an RNA sequencing analysis. Markers of the nephron progenitor (cap mesenchyme) and collecting duct progenitor (ureteric tip) were peaked by day 3 then dropped (**a**). Markers of early nephron increased by day 3, while those of mature nephron components (Proximal and distal tubule and Podocytes) started after day 3. Illustrations show expression regions (blue coloured) of each selected gene in the developing kidney (**b**). Markers of endothelial and renal interstitial cells were also increased by day 11 (**c**).

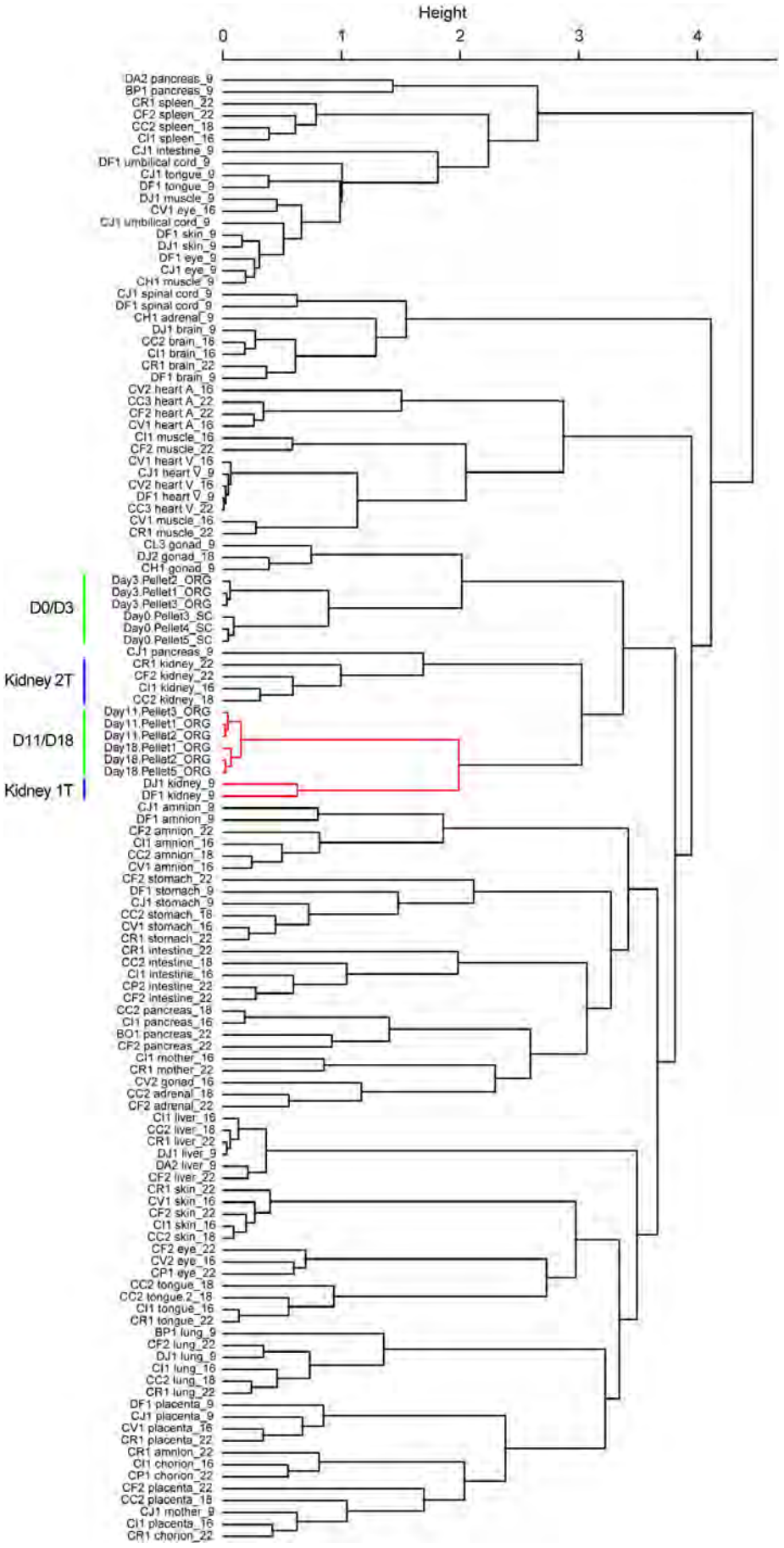

Extended Data Figure 6 | Transcriptional similarity of the kidney organoid to human fetal organs. Dendrogram showing the hierarchical clustering of day 0, 3, 11 and 18 differentiation experiments and 21 human fetal organs from first and second trimester (Gene Expression Omnibus accession number GSE66302)[15]. Sample name is composed of individual ID followed by an organ name and gestation week. For instance, 'DJ1 kidney_9' represents a kidney at ninth week gestation from individual ID: DJ1. Day 0 and 3 kidney organoids cluster with gonad, in agreement with the common origin of both gonad and kidney from the intermediate mesoderm. Day 11 and 18 kidney organoids show strongest similarity to trimester 1 human kidney. The classifier genes used for this analysis are detailed in Supplementary Table 3.

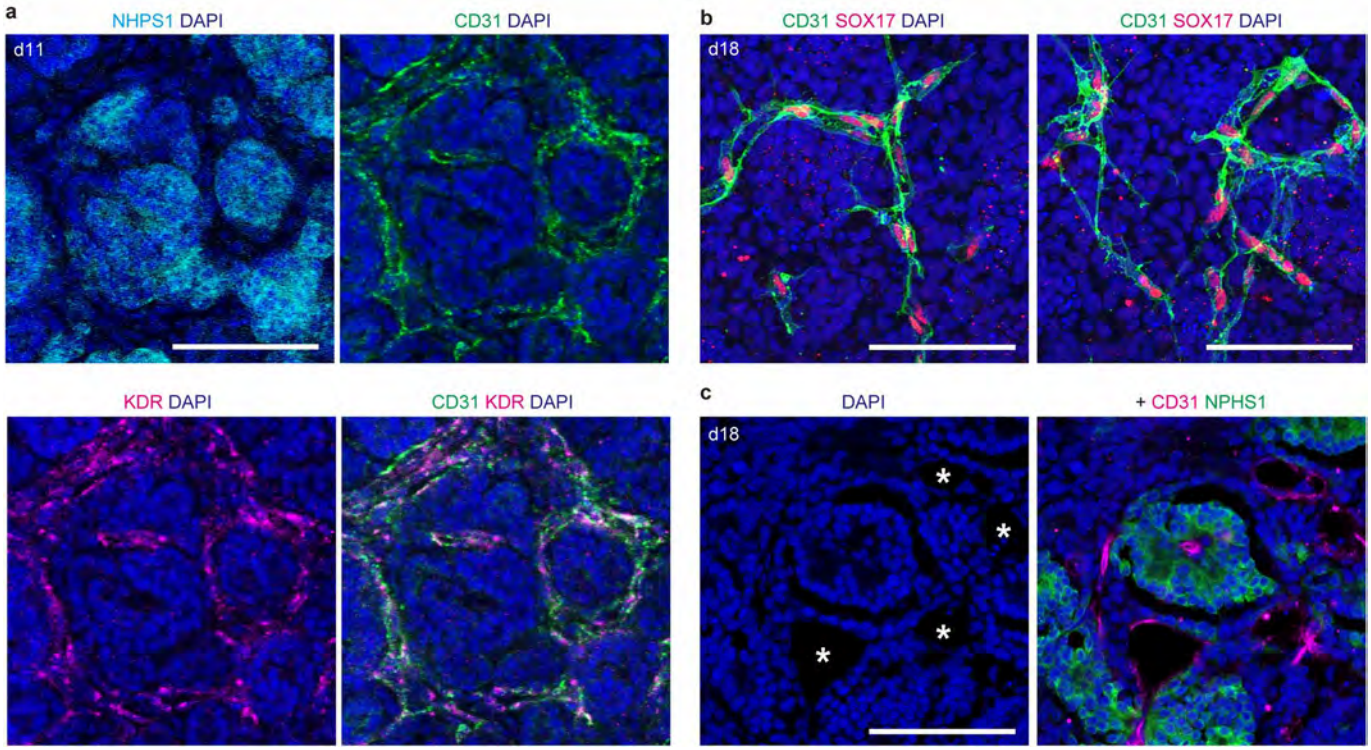

Extended Data Figure 7 | Evidence of endothelial cells in the kidney organoid. **a**, Immunofluorescence of day 11 kidney organoids showing the presence of $CD31^{+}KDR^{+}$ endothelial cells surrounding $NPHS1^{+}$ glomeruli. Scale bar, 100 μm. **b**, Two representative images demonstrating the expression of another endothelium marker SOX17 in $CD31^{+}$ endothelial cells. Scale bars, 100 μm. **c**, Immunofluorescence of day 18 kidney organoids displaying endothelia with lumen formation, as indicated by asterisks. This image also shows the endothelial invasion into a glomerulus. Scale bar, 100 μm.

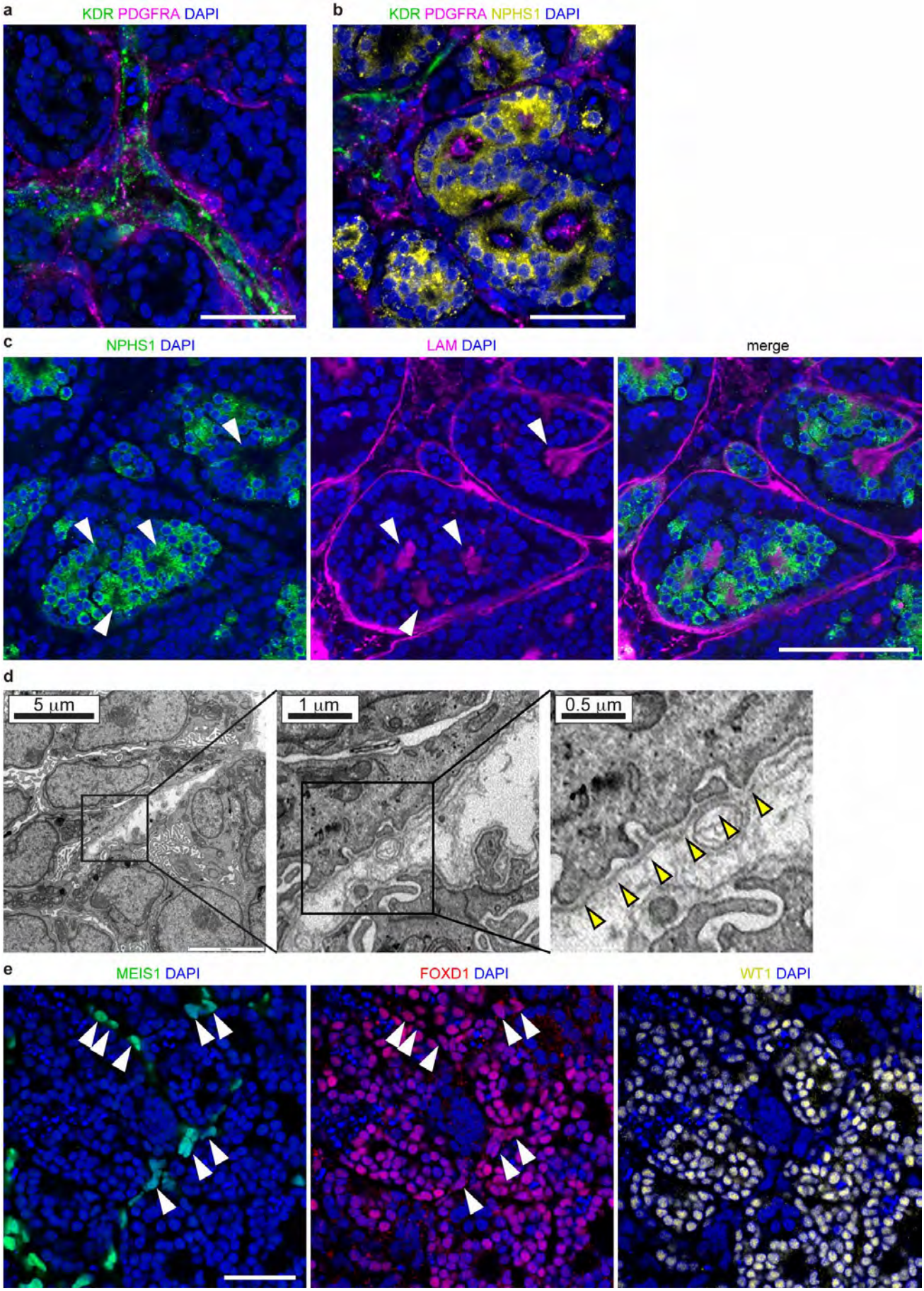

Extended Data Figure 8 | Characterization of non-epithelial structures in the kidney organoid. All images were taken from day 18 kidney organoids. **a**, $PDGFRA^+$ pericytic cells attaching on KDR^+ vessels. Scale bar, 50 μm. **b**, Some glomeruli contained $PDGFRA^+$ cells likely to represent early mesangial cells[19]. Scale bar, 50 μm. **c**, Laminin staining (LAM) demonstrates the presence of basement membrane in glomerulus structures (white arrowheads). Scale bar, 100 μm. **d**, TEM images of avascular glomeruli showing early podocytes surrounding a basement membrane (yellow arrowheads) and exhibiting foot processes on the basement membrane. **e**, Immunofluorescence showing FOXD1 expression in podocytes ($WT1^+FOXD1^+$)[18] and a subpopulation of $MEIS1^+$ interstitium (white arrowheads). This is suggestive of the presence of both cortical stroma ($FOXD1^+MEIS1^+$) and medullary stroma ($FOXD1^-MEIS1^+$). Scale bar, 100 μm.

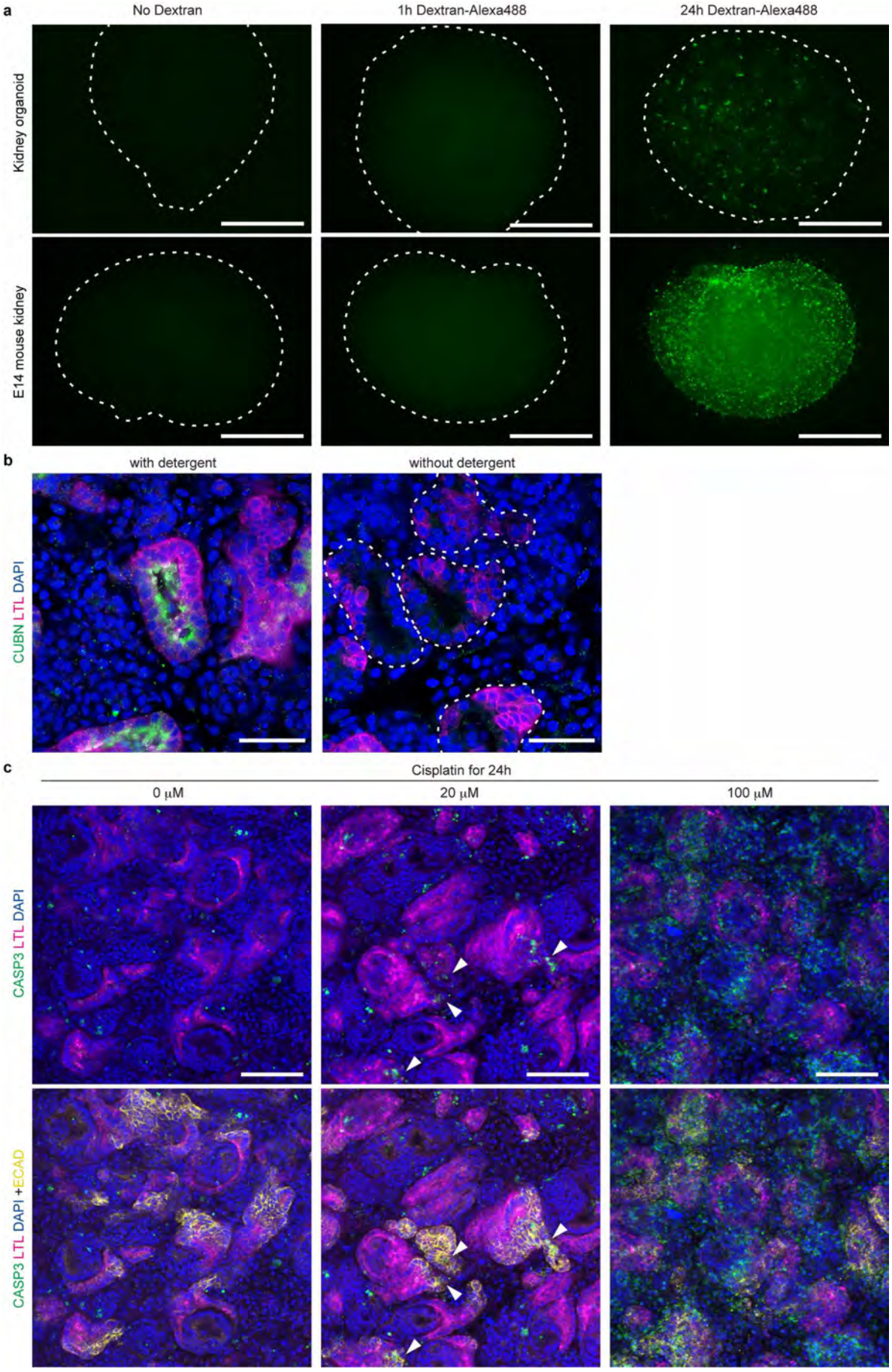

Extended Data Figure 9 | Functional assay of proximal tubule maturation within kidney organoids. **a**, Fluorescent microscopy showing the dextran uptake in both the kidney organoids and E14 mouse embryonic kidneys organ culture after 24 h presence of dextran–Alexa488 (10 $\mu g\,ml^{-1}$) in the culture medium (24 h dextran–Alexa488). 1 h incubation was insufficient for either organoids or mouse kidney explants to uptake dextran from the culture media (1 h dextran–Alexa488). No background signals were detected in a control without dextran (no dextran). Dashed line circles the organoids and kidneys. Scale bars, 1 mm. **b**, Endocytosis mediator cubilin (CUBN) was present on apical surface of the proximal tubules in kidney organoids (left panel). The same staining without detergent during the process showed the complete absence of CUBN staining on apical surface (right panel), demonstrating that the tubules within the organoids are intact. This explains the requirement for a 24 h incubation with dextran before evidence of apical uptake. Dashed line circles LTL^+ proximal tubules. Scale bars, 50 μm. **c**, Low power immunofluorescence microscopy of day 18 kidney organoids after being treated by cisplatin for 24 h. No apoptosis was observed in proximal tubules in the absence of cisplatin (0 μM, left panel). LTL^+ECAD^+ proximal tubular cell-specific apoptosis was observed only in response to either 5 μM (not shown) or 20 μM cisplatin (arrowheads in middle panel). Global cell death was observed after culture in 100 μM cisplatin (right panel). Scale bars, 100 μm.